sciendo Journal of Electrical Engineering, Vol. 76, No. 1, 2025, pp. 48-57

The influence of current on the structure of the intermetallic compound in solder alloys

Josef Skácel, Alexandr Otáhal

This paper investigates the impact of applied current on the structure of Cu_6Sn_5 and Cu_3Sn intermetallic layers and compounds within the volume of the SAC305 solder alloy. The study focuses on the transition region between a copper electrode and the solder alloy. Direct current at magnitudes of 25 A and 30 A was applied for durations of 30 and 90 minutes, alongside samples fabricated without current application. After the samples were prepared, the surfaces were refined through sanding and subsequent polishing with diamond pastes. To enhance the quality of data obtained from these samples, the surfaces were etched, improving the visibility of their microstructure. Statistical analysis of the intermetallic layer thickness at the Cu electrode–solder alloy interface was conducted. The results revealed a significant influence of applied current on the width of the intermetallic layers. Measurements demonstrated a polarity-dependent effect on the layer thickness, that samples formed under current exhibiting substantially thicker layers at the positive electrode compared to the negative electrode. Additionally, the samples with applied current showed a significant increase in the size of intermetallic compounds within the solder alloy, reaching dimensions of several millimeters. The final part of the research involved elemental analysis to confirm the composition of the intermetallic compounds. This analysis validated the presence of Cu_6Sn_5 and Cu_3Sn.

Keywords: SAC305, intermetallic compound, intermetallic layer, Cu_6Sn_5, Cu_3Sn

1 Introduction

Soldering is a fundamental process in the creation of electronic connections. During soldering, solder alloys are used, and their properties and behavior are critical factors in determining the quality of these connections. From this perspective, it is essential to understand the factors influencing the behavior of solder alloys under various conditions and their impact on the resulting soldered joint. One notable approach involves the use of ultrasound, which is applied as a method to create soldered joints using an ultrasonic tip. This technique enables the soldering of incompatible materials that cannot be joined using conventional methods. Research has demonstrated that during the formation of a soldered joint, the application of ultrasonic vibrations at frequencies between 28 and 35 kHz during solidification leads to a refinement of the joint's microstructure. Additionally, it influences the orientation of β-Sn dendrites, aligning them perpendicularly to the soldering surface. When ultrasound was applied with a power of 10 W for 6 seconds, a significant increase in the intermetallic compound Ag_3Sn was observed [1].

Another method for influencing solder alloys is the application of a magnetic field. Studies have confirmed that a static magnetic field can promote the formation of high-quality single crystals and affect phase transformations [2].

A currently popular area of research involves the impact of an applied current during the solidification of solder alloys. It has been observed that applying a current as low as 2.5 A to a droplet of solder alloy significantly increases its wettability. The applied current also influences the growth of the intermetallic layer, particularly in relation to the current's direction. Additionally, the Marangoni effect was observed under these conditions, enhancing the mixing of the solder alloy and promoting greater transport of intermetallic compounds. By applying an electric current, the angle between peaks of the intermetallic layer within a SnFe alloy can be reduced [3-4].

The orientation of β-Sn grains is particularly crucial for joint quality, especially in terms of electromigration resistance. It has been confirmed that the orientation of β-Sn grains can be controlled. From the perspective of cubic orientation, diffusion coefficients of copper atoms are 500 times slower along the a and the b directions compared to the c direction [5].

The solder alloy volume also affects the resulting microstructure. Larger solder volumes result in thicker intermetallic layers [6].

This study focuses on the possibility of controlling the growth of intermetallic compounds in solder alloys through the application of an electric current via copper electrodes. The work aims to explore the potential for modifying the growth and surface of intermetallic layers and the intermetallic compounds within the solder alloy volume.

Department of Microelectronics, Brno University of Technology, Technologická 10, Brno, Czech Republic
Josef.Skacel@vutbr.cz

https://doi.org/10.2478/jee-2025-0005, Print (till 2015) ISSN 1335-3632, On-line ISSN 1339-309X

2 Methodology

The experimental setup was designed to meet the requirements of high-temperature resistance and the ability to melt a specific volume of solder alloy without wetting the material. For this purpose, a quartz tube (SiO_2) was selected due to its excellent high-temperature resistance, allowing it to withstand elevated temperatures without altering its shape or properties. Quartz glass is also chemically inert, making it unlikely to contaminate or react with other substances during the experiment. Another feature of quartz glass is its non-wettability by the solder alloy, which ensures that the alloy can be easily removed from the tube afterward. The transparency of the apparatus, inherent to quartz glass, provides the advantage of observing the experiment, while its low thermal expansion facilitates the easy removal of the cooled solder ingot from the tube. For the heating element, Kanthal resistance wire (1.28 Ω/m) was selected. Kanthal is commonly used in heating elements due to its malleability, high thermal resistance, and durability. The Kanthal wire is com-posed of iron, chromium, aluminum, and trace amounts of cobalt. Upon heating, an oxide layer forms on the surface of the wire, acting as a protective barrier to prevent further reactions. The wire was wound around a rod with a smaller diameter than the quartz tube, ensuring that the heating element could be mounted with slight tension to maintain good thermal contact with the tube, even during thermal expansion.

Temperature simulations were performed in ANSYS Workbench 2024 R1, focusing on the uniformity of temperature distribution across the solder ingot, taking the winding geometry into account. For sealing the ends of the quartz tube, CERESIT CS 28 Thermo Resistant silicone was chosen, which can withstand temperatures up to 315 °C. Through these seals, copper electrodes were inserted. The experimental setup and a 3D model of the assembly are shown in Fig. 1.

Fig. 1. Experimental setup for sample preparation and 3D model

Prior to creating the ingots, simulations were performed using ANSYS Electronics Desktop 2024 R1 in the Maxwell 3D – DC Conduction module to calculate the theoretical current density in the ingots. Current density is a critical parameter influencing the internal structure of the ingot. During the ingot fabrication, a power source connected to the Kanthal wire was set to 13.4 V and 5.3 A for samples created without an applied current on the copper electrodes. For samples with an applied current, a lower current was used to account for the heating of the solder alloy caused by the applied current. The appropriate current levels were determined experimentally. Temperature measurements were made possible by the application of an emissive spray with a measured emissivity of 0.912, measured at an angle of 30°. After turning on the Kanthal heating winding, solder alloy SAC 305 was gradually added until the quartz tube was sufficiently filled and sealed with a top plug. Once the steady state temperature was achieved, the experimental timer was started. For samples with applied current, the power source for the copper electrodes was set to 25 A or 30 A.

The ingots were created over durations of 30 minutes and 90 minutes, both for samples with and without applied current. After these periods, the Kanthal heating source was turned off. For samples without applied current, the cooling profile was adjusted to match that of the current-applied samples. Due to the differing thermal expansion properties of the solder alloy and quartz tube, the cooled ingots could be easily removed. After the ingots were created, sample preparation for structural inspection was carried out. The first step was manual grinding due to the size of the ingots. Samples were ground to approximately half their thickness, exposing both electrode sides. Grinding was performed using abrasive papers with grit sizes of 80, 400, 800, and 1500. This was followed by polishing with diamond pastes applied to lint-free cloths, using particle sizes of 5 μm, 3.5 μm, 1.5 μm, 1 μm, and 0.25 μm. However, at the smallest particle size (0.25 μm), the physical properties of the solder alloy caused surface smearing, obscuring certain details. To reveal information concealed beneath this surface layer, the samples underwent etching using a solution of ethanol, HNO_3, and HCl in a ratio of 94%, 4%, and 2%, respectively. This etchant effectively exposed the metallographic structure of β-Sn dendrites, grain orientation, and intermetallic layer boundaries and compounds. Following etching, optical inspection of the surface was conducted using a Zeiss Axio Imager.A2m microscope, which captured images of the intermetallic layer at the interface between the copper electrodes and the solder alloy.

These images were processed using ImageJ software to measure the intermetallic layer's area and length. The data was subsequently analyzed using the formula for calculating the Mean Structural Layer Width (MSL):

$$MSL = \frac{A}{L} \quad (\mu m) \qquad (1)$$

Another part of the research involved surface inspection and elemental composition analysis using Energy Dispersive X-ray Spectroscopy (EDX) with a Tescan MIRA II SEM microscope. The purpose was to determine the composition of intermetallic layers and compounds.

3 Results

In the experiments, Kanthal wire was wound with uniform spacing of 5 mm, completing 28 turns. To study the behavior of the system, simulations were performed using ANSYS Workbench 2024 R1. The materials used in the simulation were chosen to match those used in the experiments, namely Kanthal wire, SAC 305 solder alloy, and quartz glass. The initial simulation conditions were carefully configured to ensure accurate results. The automatically generated mesh required refinement, as the default settings led to inaccuracies. For the Kanthal wire, the mesh was set to MultiZone with a fineness of 0.5 mm. The Internal Heat Generation parameter was adjusted so that the system would reach a target temperature range of 320-330 °C. The results of the simulation revealed significant temperature gradients in the system shown in Fig. 2.

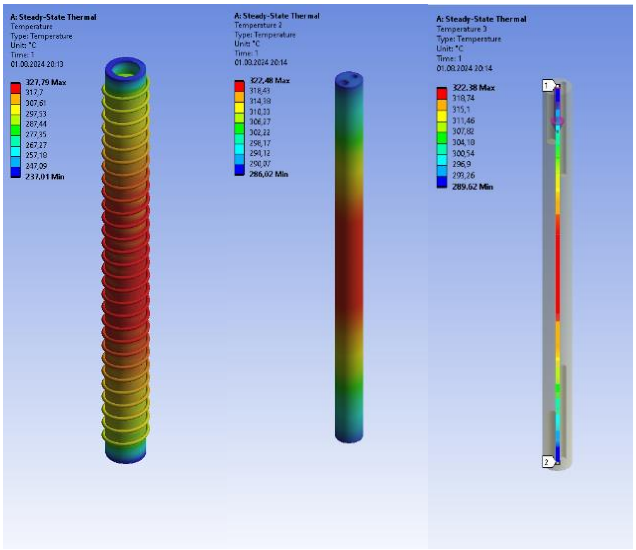

Fig. 2. Simulation of temperature distribution in the assembly

The steady-state temperature distribution of the entire assembly showed a difference of 90.8 °C, primarily due to greater heat dissipation at the ends of the quartz tube, which led to localized cooling. Within the SAC 305 solder ingot, a temperature difference of 36.5 °C was observed. Additionally, a temperature profile along a point line from the center of the ingot's top to its bottom revealed a gradient of 32.8 °C. Such pronounced temperature differences between the edges and the central region of the system present a challenge for the experiment. To ensure reliable results, it is necessary to reduce this thermal gradient to the lowest possible value.

The non-homogeneous temperature field significantly impacts the formation of the internal structure, potentially affecting grain size, cubic orientation, the growth of intermetallic compounds, and the overall resulting structure of the solder alloy. The temperature gradient is also a crucial parameter influencing the formation of the intermetallic layer, as noted in the publication [7]. When testing the influence of a temperature gradient across a soldered joint, it was concluded that the intermetallic layer (IML) exhibited greater growth on the cooler end of the solder joint compared to the warmer side. This phenomenon is attributed to thermomigration of copper atoms from the hotter side to the cooler side.

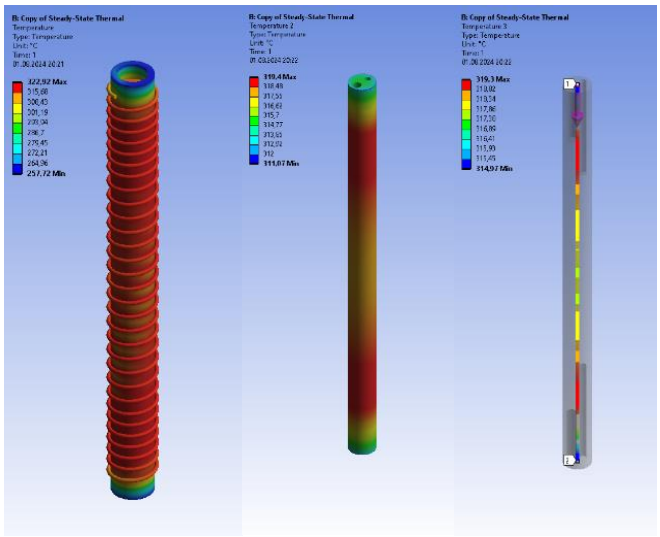

Fig. 3. Optimized winding for improved temperature distribution

Figure 3 illustrates the temperature distribution from a systemic perspective, where the difference between the minimum and maximum temperatures is 65.2 °C. This calculation includes the temperature at the ends of the quartz tube on both sides, where the minimum temperature does not affect the experiment. The second part of the figure depicts the temperature gradient within the volume of the SAC 305 solder alloy ingot, showing a resulting temperature difference of 8.4 °C. The final part of the temperature simulation highlights the tempe-

rature difference along a line within the simulated ingot. In this case, the difference was approximately 4.3 °C.

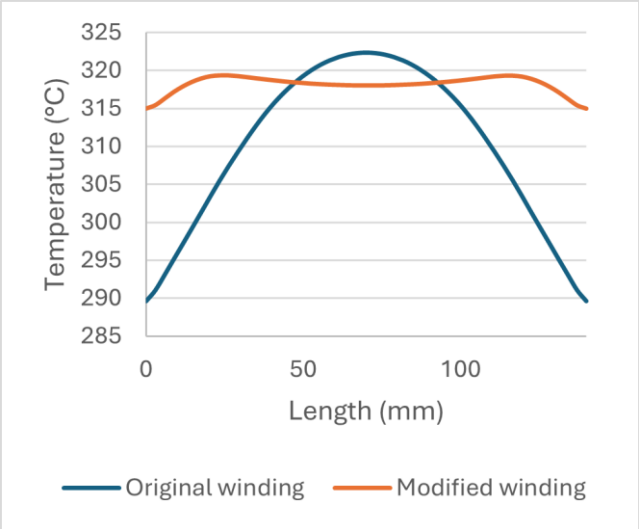

Fig. 4. Temperature distribution comparison in the solder alloy

Figure 4 shows the temperature distribution based on the line profile for both winding configurations. Here, a significant reduction in the temperature gradient between the minimum and maximum temperatures in the simulation was observed. This simulation aims to achieve the lowest possible temperature gradient at both ends of the testing assembly, particularly within the solder alloy volume. A subsequent simulation focused on the current density distribution in the solder ingot. Current density and temperature are critical parameters influencing the phenomena under investigation. The model used was identical to the previous simulation, excluding the heating components, and the modeling software was Ansys Electronics Desktop 2024 R1 in the Maxwell 3D – DC Conduction module. The first step involved setting the materials for the model: copper for the electrodes and SAC 305 solder alloy. Initial conditions included applying current to a copper electrode with a 3 mm diameter and defining the current direction. The analysis settings specified a maximum of 10 calculation passes, a 1% error tolerance, a 30% mesh refinement per pass, a minimum of 2 passes, and at least 1 convergence step per iteration. The evaluation focused on current density distribution within the ingot cross-section, centered along the ingot. For numerical analysis, line profiles were taken between electrodes with diameters of 3 mm and 2 mm. Graphs were plotted for different current levels, demonstrating that current is diverted from the 3 mm electrode through the 2 mm electrode into the ingot volume. The results of this simulation are shown in Fig. 5.

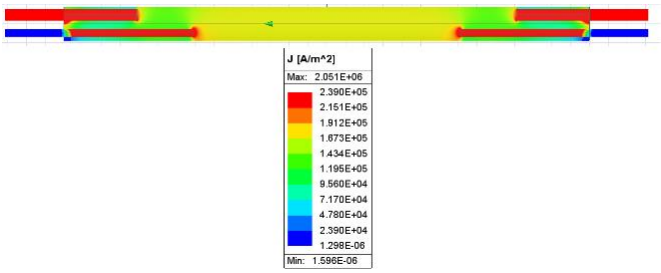

Fig. 5. Simulation of current density in the entire sample volume

To provide precise numerical values for current density, a graph was plotted for various applied current levels at the electrodes. The measured area was the distance between two opposing current electrodes, as shown in Fig. 6.

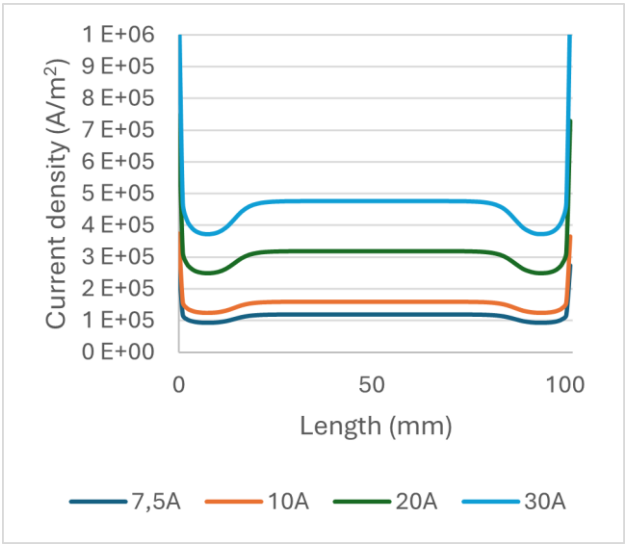

Fig. 6. Numerical values of current density between electrodes

Sample preparation involving grinding, polishing, and surface etching (as described in the methodology), the intermetallic layer was imaged, and statistical analysis of its thickness was performed. This included calculating the Mean Layer Thickness (MSL) for samples created without current and with applied current for durations of 30 and 90 minutes. From the captured images of the intermetallic layer (Fig. 7), masks were created using the ImageJ software (Fig. 8), and the MSL parameter was calculated based on these measurements.

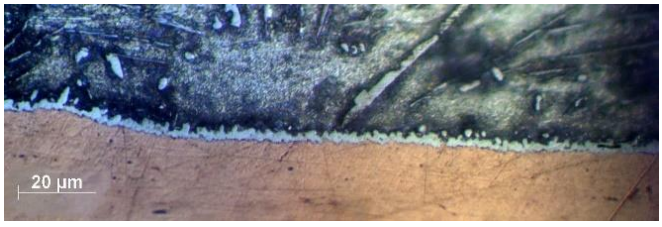

Fig. 7. Intermetallic layer at the copper electrode-solder alloy interface

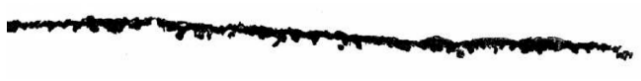

Fig. 8. Mask created in ImageJ software

The processed data for samples without current and with current (30 min and 90 min durations) were plotted in box plots. Figure 9 displays the mean MSL values, highlighting calculated parameters. For the ingot without current, the maximum mean IML thickness was 3.1 µm, and the minimum was 2.59 µm. The upper quartile was 3.07 µm, and the lower quartile was 2.65 µm, with a mean value of 2.87 µm and a median of 2.9 µm. For the ingot with 25 A applied current, the maximum mean thickness was 3.35 µm, and the minimum was 2.47 µm. The upper quartile was 3.28 µm, and the lower quartile was 2.59 µm. The mean was 2.95 µm, and the median was 2.98 µm. The data reveal that while the values are similar, the thickness range for the 25 A ingot increased by approximately 68% compared to the ingot without current.

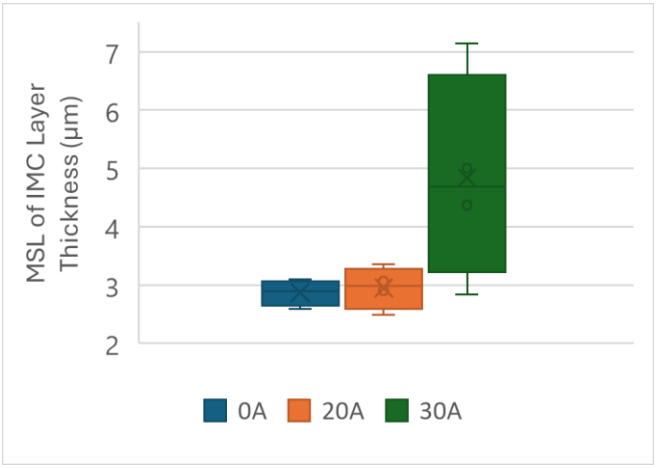

Fig. 9. MSL of the intermetallic layer thickness

In the case of the ingo with 30 A applied current, the maximum mean thickness was 7.14 µm, and the minimum was 2.837 µm. The upper quartile was 6.605 µm, and the lower quartile was 3.22 µm, with a mean value of 4.84 µm and a median of 4.69 µm. This represents a significant change in MSL compared to ingots 1 and 2. The range of MSL values was much larger for this ingot, likely due to the influence of current during remelting and the possible effect of heat generated by the applied current on the intermetallic layer thickness.

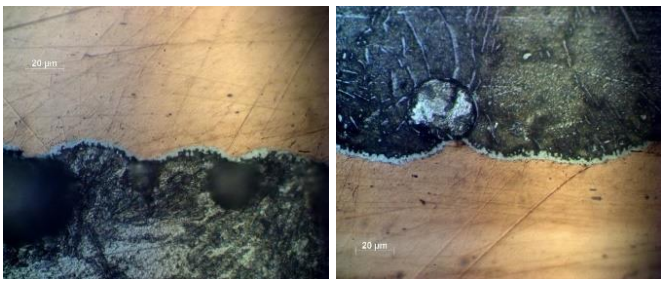

Fig. 10. IMC layer of a sample created without current: bottom and top electrodes

Figure 10 shows the bottom and top electrodes fabricated without applied current. During imaging, voids appeared in certain areas, which affected the IMC layer's width or caused deformation. Additionally, the diffusion of the copper pad into the solder alloy was less pronounced at these locations.

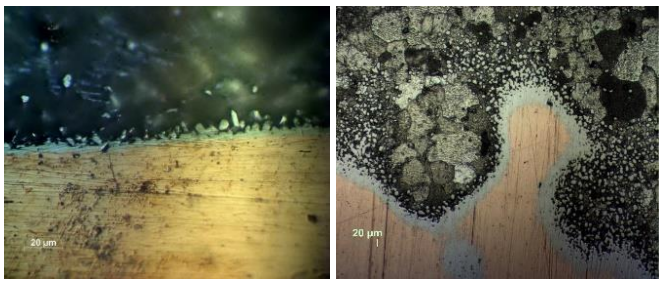

Fig. 11. IMC layer of a sample created with current: negative and positive polarities

Figure 11 shows ingot created with current, specifically the Cu-SAC305 interface fabricated under a 30 A current. The image shows the current positive electrode and its outer region. The IMC layer diffuses significantly into the solder alloy volume, especially near the positive polarity electrode. According to the publication [4], this phenomenon results from the additional energy introduced by the current, causing a thermal gradient and triggering the Marangoni effect. Furthermore, the applied current facilitates easier IMC layer formation and increases its surface roughness. The publication [3] states that current flow during IMC layer formation alters the layer's morphology, creating taller peaks with lower interfacial angles than those seen without current. These peaks may diffuse more readily into the solder alloy. Conversely, at the negative electrode of ingot created with current, IMC diffusion into the solder volume was less pronounced. As noted in interfacial reactions in molten state micro solder joints under current stressing, current application during IMC formation enhances layer growth on both polarities, with the extent depending on electron flow direction.

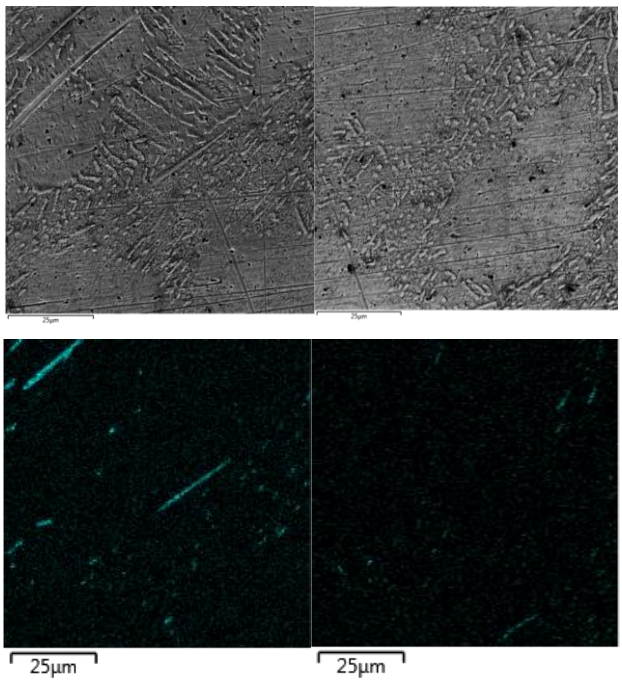

Fig. 12. SEM image of ingot without current, bottom and top regions, and corresponding Cu content by EDX

Figure 12 shows SEM images of an ingot fabricated without applied current, focusing on the bottom and top regions along with the copper distribution. The bottom region contains more IMC compounds, specifically Cu_6Sn_5, due to the prolonged immersion of the bottom electrode in liquid solder during the sequential addition of solder alloy. EDX line scans confirmed the presence of IMC compounds both in the solder volume and on the interface.

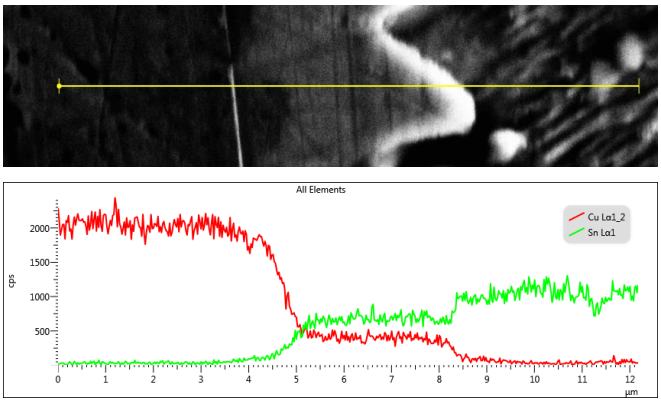

Fig. 13. EDX of the IMC layer

Figure 13 presents the elemental composition of the IMC layer at the Cu-SAC305 interface. Based on EDX measurements, the Cu_6Sn_5 phase consists of approximately 40% copper and 60% tin by weight, consistent with its stoichiometric ratio. Measurements confirmed the material composition of this intermetallic compound.

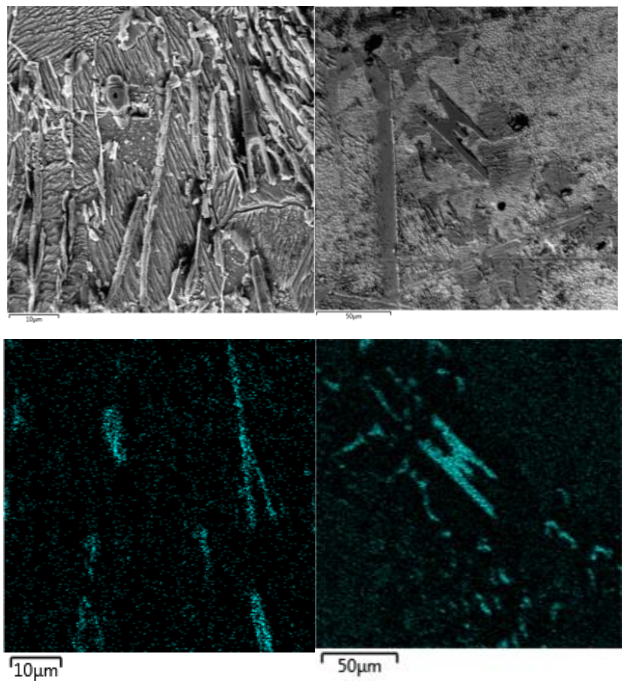

Fig. 14. SEM image of ingot with 30 A: negative and positive polarities, and Cu content by EDX

Figure 14 highlights the surface structure of an ingot created with 30 A. Analysis confirms that the observed IMC compounds are predominantly Cu_6Sn_5. The proportion of IMC compounds is higher in samples fabricated with current compared to those without. The applied current influenced diffusion, with Cu atoms migrating from the negative to the positive electrode. The IMC shapes formed without current were elongated and simple, while those formed with current were more complex and significantly larger. A subsequent experiment extended the ingot fabrication time to 90 minutes to investigate whether longer durations lead to new phases, such as Cu_3Sn, or further IMC layer growth.

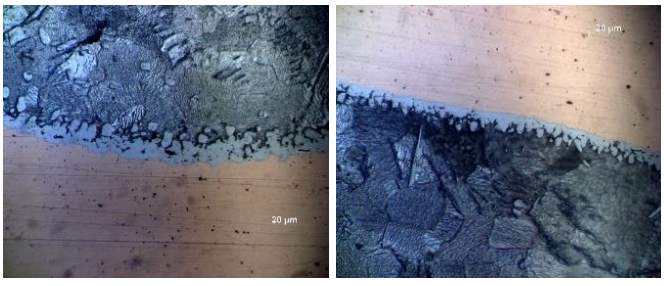

Fig. 15. SEM image of ingot without current, bottom and top regions

Figure 15 shows the SEM image of the bottom region of an ingot fabricated without current. The presence of a Cu_3Sn layer was confirmed via EDX analysis. However, the Cu_3Sn layer was not uniformly distributed, with its

width varying between 0-2 µm. On the top side, the Cu_3Sn layer width was barely measurable, reaching a maximum of 0.5 µm. Therefore, it was not possible to process these layers statistically.

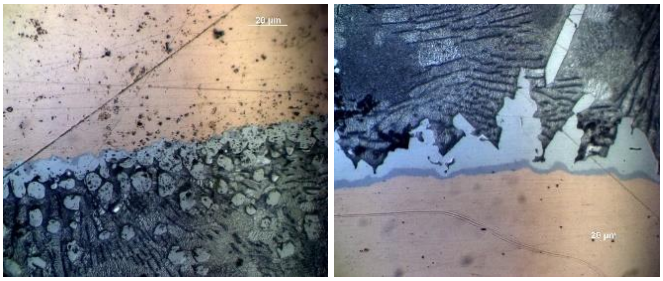

Fig. 16. SEM image of ingot created with 30 A negative and positive polarities

Figure 16 illustrates the SEM image of the positive electrode region in an ingot fabricated with a 30 A current. The Cu_3Sn IMC layer width ranged from 2 to 5.5 µm and was more consistent across the interface compared to the sample fabricated without current. Notable differences in morphology were observed in Cu_6Sn_5 phases, which exhibited non-homogeneous widths and shapes, likely influenced by electron flow. Large, isolated IMC particles, primarily Cu_6Sn_5, were often observed near the positive electrode, suggesting that excessive growth at certain points was caused by the presence of nearby IMC clusters. These particles were hexagonal in shape and featured internal cavities. The reason for the creation of these structures can be due to the possibility of Cu_6Sn_5 rods being affected by the flow of electrons, which can cause anisotropic nucleation and growth behavior of Cu_6Sn_5 [8].

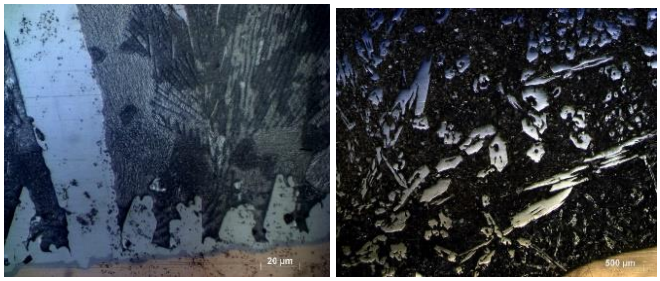

Fig. 17. Notable IMC compound

Figure 17 shows the enormous growth of the intermetallic layer at one point. This phenomenon occurred frequently in the samples, and it is this phenomenon that caused such a large scatter of values on the plot of the mean intermetallic layer width. A possible reason for this phenomenon is when a large intermetallic particle is diffused and formed in the volume of the soldering alloy. These large intermetallic particles that moved towards the positive electrode of the formed sample can be seen in Fig. 17. These intermetallic compounds are Cu_6Sn_5 and as can be seen by the scale of the formed image the size of these compounds is on the order of 100 µm to several millimeters in size. From this phenomenon, it can be inferred that the disproportionate growth of the intermetallic compound at certain locations in the intermetallic layer was due to this occurrence in the vicinity of the positive electrode. It can also be observed that some intermetallic compounds have a hexagonal shape with a cavity inside the structure. Also in this part, there was a statistical calculation of the width of the intermetallic layer at the transition of the Cu surface and the SAC305 solder alloy.

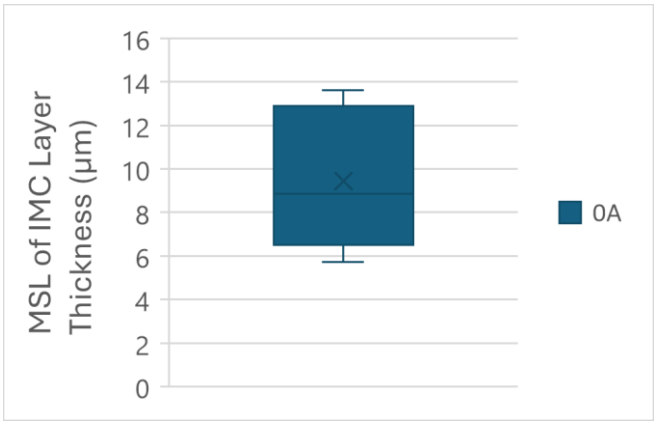

Fig. 18. Mean IMC layer thickness in ingot without current

Figure 18 shows the mean thickness of the IMC layer in an ingot fabricated without current. The layer width ranged from 5.8 to 13.6 µm, with the bottom electrode showing double the width of the top electrode due to the fabrication process.

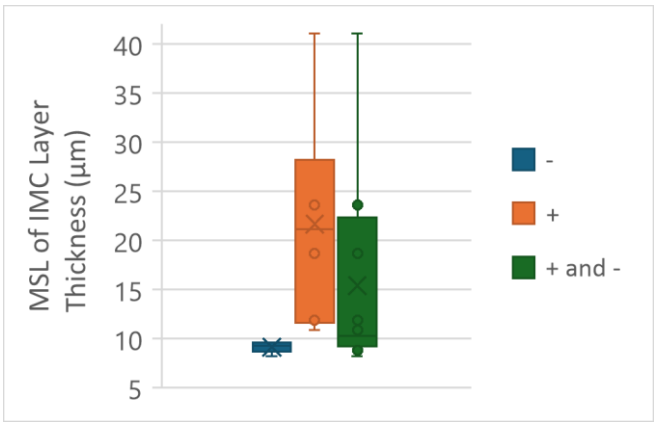

Fig. 19. Mean IMC layer thickness in ingot with 30 A

From the perspective of the average intermetallic layer width, the sample created under the influence of current provides a clear indication of the impact of the

applied current. Figure 19 presents a graph depicting the average width of the intermetallic layer. Due to significant differences between the electrodes, the graph was divided into sections for the positive and negative electrodes as well as their combination. The graph demonstrates that the negative electrode exhibits a relatively low intermetallic layer width, ranging between 8-9.5 μm. This phenomenon can be attributed to the continuous diffusion of the intermetallic layer into the solder alloy volume under the influence of electron flow. The second box plot, shown in orange, represents the positive electrode of the sample. Here, a notable growth of the intermetallic layer on the positive electrode is observed. This phenomenon aligns with the previous assertion that the direction of electron flow induces diffusion from the negative electrode, including the intermetallic layer, and subsequently transports these compounds and materials to the positive electrode.

The subsequent section compares the surface structure and the transition between the copper pad and the intermetallic Cu_3Sn layer. Figures 20 and 21 illustrate the transitions observed between materials on the negative electrode and subsequently on the positive electrode, with a layer length of 170 μm. Based on these observations, it can be concluded that under the influence of electron flow, the negative electrode undergoes a more pronounced local diffusion of the intermetallic layer into the copper pad and further into the solder alloy volume. In contrast, the surface of the intermetallic layer on the positive electrode does not exhibit such a rough interface in the copper-Cu_3Sn transition.

Fig. 20. Transition between the copper pad and Cu_3Sn on the negative electrode (l = 170 μm)

Fig. 21. Transition between the copper pad and Cu_3Sn on the positive electrode (l = 170 μm)

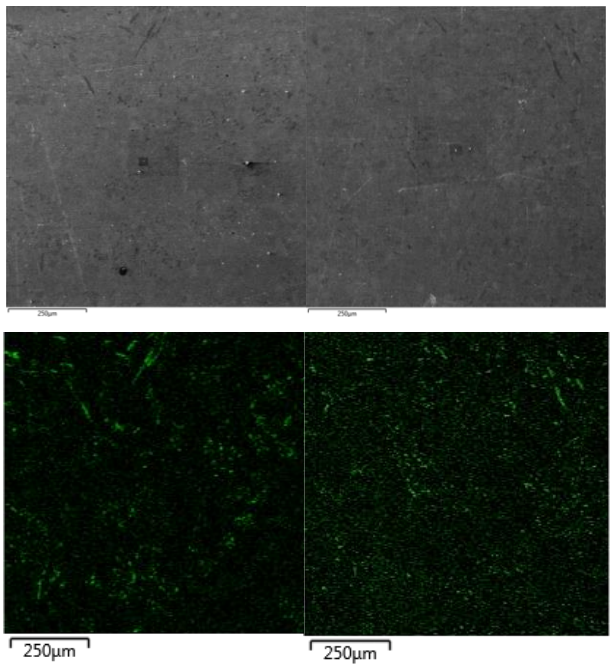

Fig. 22. SEM image of an ingot created without applied current (90 min), bottom/top surfaces, and EDX mapping of copper distribution

Figure 22 shows intermetallic compound regions within the solder alloy volume, appearing darker than the solder matrix. Compared to an ingot fabricated without current under a 30-minute thermal profile, this sample, processed under identical conditions but for 90 minutes, exhibits significant differences in the content and size of the intermetallic compounds. In this case, intermetallic compounds approximately 150 μm in size were observed.

Figure 23 shows the region near the negative electrode, where large intermetallic Cu_6Sn_5 compounds with a hexagonal shape are present. Near the positive electrode of the ingot produced under current flow, a substantial amount of intermetallic Cu_6Sn_5 compounds can be seen, forming clusters around the positive electrode. The influence of electron flow induced the transport of these compounds toward the positive electrode. The intermetallic layer widths at the copper-solder alloy interface, presented in the previous section, were likely influenced by the compounds shown in Fig. 23. Fundamentally, this reflects the accelerated diffusion of elements into the solder alloy volume and their subsequent transport. In both cases, Cu_3Sn was not detected in the solder alloy volume.

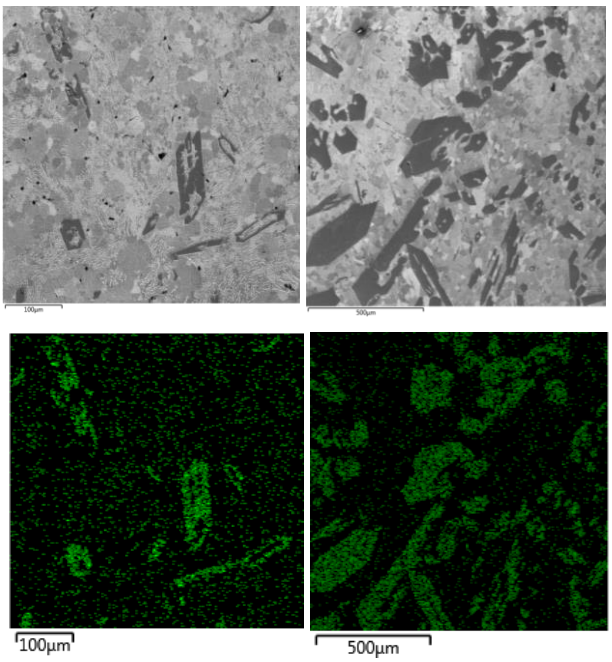

Fig. 23. SEM image of an ingot fabricated with an applied current of 30 A, negative and positive electrodes, and EDX mapping of copper distribution

4 Discussion

This study examined the influence of electric current on the structure of soldered joints, focusing on the intermetallic layer at the copper pad-SAC solder alloy interface and intermetallic compounds within the solder alloy volume. The results confirmed the ability to control the size of the Cu_6Sn_5 intermetallic layer at the interface and the Cu_3Sn intermetallic compound in the same region. In both cases, the applied current significantly affected the size of these layers. For samples fabricated under current application, a notable difference in intermetallic layer thickness was observed between the positive and negative electrodes. The layer at the negative electrode was thinner and more homogeneous, while the layer at the positive electrode exhibited larger thickness and sharper angles between peaks also confirmed by the research [3]. Statistical analysis of the Mean Structural Layer (MSL) values demonstrated that samples produced with current had intermetallic layers several times thicker compared to those fabricated without current. The layer thickness also showed a strong dependence on polarity. The negative electrode exhibited even thinner layers than the non-current samples, while the positive electrode displayed substantially thicker layers this behavior is confirmed by [7]. A polarity-dependent difference in the flatness of the Cu_3Sn layer at the copper pad interface was also identified. The negative electrode showed a coarser structure due to enhanced material diffusivity along the electron flow direction [9, 10]. Conversely, the Cu_3Sn layer on the positive electrode was more homogeneous throughout. Additionally, the formation of large intermetallic compounds, reaching sizes of several millimeters, was observed within the solder alloy volume, predominantly clustering near the positive electrode. The composition of these intermetallic layers and compounds was verified using EDX elemental analysis. Future research will focus on the behavior of intermetallic layers and compounds under alternating current conditions.

5 Conclusions

Findings of this work were as follows:

- Influence of current on intermetallic layers: Electric current significantly affects the thickness and morphology of Cu_6Sn_5 and Cu_3Sn intermetallic layers at the copper pad-solder alloy interface.
- Polarity dependence: At the positive electrode, the intermetallic layers were notably thicker with sharper angles between peaks, whereas at the negative electrode, the layers were thinner and more homogeneous. The direction of electron flow (electron wind) facilitated material diffusion, resulting in a coarser layer structure at the negative electrode and more homogenous at the positive electrode.
- Statistical differences in layer thickness: Samples produced under the influence of current exhibited intermetallic layer thicknesses several times greater than those of samples without current.
- Formation of large particles in the alloy volume: Intermetallic compounds reaching sizes of several millimeters were observed within the solder alloy volume, predominantly clustering near the positive electrode.

Acknowledgements

The article was supported by project no. FEKT-S-23-8162, Modern micro- and nanoelectronics for future. Our thanks belong also to the company NeVo (Shenmao Technology Inc.) as a supplier of soldering materials for this work.

References

[1] H. Cai, W. Lin, M. Feng, T. Zheng, B. Zhou, and Y. Zhong, "Review on Eutectic-Type Alloys Solidified under Static Magnetic Field", *Crystals*, vol. 13, no. 6, 2023. doi: 10.1016/j.ultsonch.2016.06.039.

[2] H. Cai, W. Lin, M. Feng, T. Zheng, B. Zhou, and Y. Zhong, "Review on Eutectic-Type Alloys Solidified under Static Magnetic Field", *Crystals*, vol. 13, no. 6, 2023. doi: 10.3390/cryst13060891.

[3] P. Shen, Y. Gu, N. -N. Yang, R. -P. Zheng, and L. -H. Ren, "Influences of electric current on the wettability and interfacial microstructure in Sn/Fe system", *Applied Surface Science*, vol. 328, pp. 380-386, 2015. doi: 10.1016/j.apsusc.2014.12.080.

[4] Y. Gu, P. Shen, N. -N. Yang, and K. -Z. Cao, "Effects of direct current on the wetting behavior and interfacial morphology between molten Sn and Cu substrate", *Journal of Alloys and Compounds*, vol. 586, pp. 80-86, 2014. doi: 10.1016/j.jallcom.2013.10.021.

[5] M. N. Bashir, S. U. Butt, M. A. Mansoor, N. B. Khan, S. Bashir, Y. H. Wong, T. Alamro, S. M. Eldin, and M. Jameel, "Role of Crystallographic Orientation of β-Sn Grain on Electromigration Failures in Lead-Free Solder Joint: An Overview", *Coatings*, vol. 12, no. 11, 2022. doi: 10.3390/coatings12111752.

[6] M. I. I. Ramli, M. A. A. M. Salleh, M. M. A. B. Abdullah, N. S. M. Zaimi, A. V. Sandu, P. Vizureanu, A. Rylski, and S. F. M. Amli, "Formation and Growth of Intermetallic Compounds in Lead-Free Solder Joints: A Review", *Materials*, vol. 15, no. 4, 2022. doi: 10.3390/ma15041451.

[7] J. Feng, C. Hang, Y. Tian, B. Liu, and C. Wang, "Growth kinetics of Cu6Sn5 intermetallic compound in Cu-liquid Sn interfacial reaction enhanced by electric current", *Scientific Reports*, vol. 8, no. 1, 2018. doi: 10.1038/s41598-018-20100-1.

[8] T. Laurila, V. Vuorinen, and J. K. Kivilahti, "Interfacial reactions between lead-free solders and common base materials", *Materials Science and Engineering: R: Reports*, vol. 49, no. 1-2, pp. 1-60, 2005. doi: 10.1016/j.mser.2005.03.001.

[9] J. F. Zhao, C. Unuvar, U. Anselmi-Tamburini, and Z. A. Munir, "Kinetics of current-enhanced dissolution of nickel in liquid aluminum", *Acta Materialia*, vol. 55, no. 16, pp. 5592-5600, 2007. doi: 10.1016/j.actamat.2007.06.016.

[10] Y. -D. Lu, X. -Q. He, Y. -F. En, X. Wang, and Z. -Q. Zhuang, "Polarity effect of electromigration on intermetallic compound formation in SnPb solder joints", *Acta Materialia*, vol. 57, no. 8, pp. 2560-2566, 2009. doi: 10.1016/j.actamat.2009.02.015.

Received 17 November 2024